Highly Angiogenic Peptide Nanofibers

Vivek A. Kumar, Nichole L. Taylor, Siyu Shi, Benjamin K. Wang, Abhishek A. Jalan, Marci K. Kang, Navindee C. Wickremasinghe, and Jeffrey D. Hartgerink*

Department of Chemistry and Department of Bioengineering, Rice University Mail Stop 602, 6100 Main Street, Houston, Texas 77030, United States

ABSTRACT

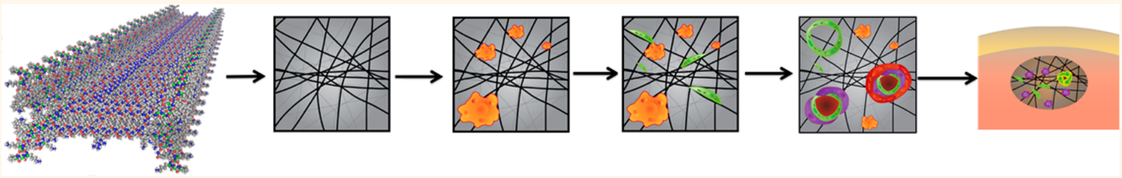

Major limitations of current tissue regeneration approaches using artificial scaffolds are fibrous encapsulation, lack of host cellular infiltration, unwanted immune responses, surface degradation preceding biointegration, and artificial degradation byproducts. Specifically, for scaffolds larger than 200−500 μm, implants must be accompanied by host angiogenesis in order to provide adequate nutrient/waste exchange in the newly forming tissue. In the current work, we design a peptide-based self-assembling nanofibrous hydrogel containing cell-mediated degradation and proangiogenic moieties that specifically address these challenges. This hydrogel can be easily delivered by syringe, is rapidly infiltrated by cells of hematopoietic and mesenchymal origin, and rapidly forms an extremely robust mature vascular network. Scaffolds show no signs of fibrous encapsulation and after 3 weeks are resorbed into the native tissue. These supramolecular assemblies may prove a vital paradigm for tissue regeneration and specifically for ischemic tissue disease.

KEYWORDS: self-assembly · supramolecular chemistry · multidomain peptide · angiogenesis

Fundamentally, tissue will not grow or repair from a wound if there is not suitable blood supply to carry out basic exchange of oxygen, nutrients, and waste material. Similarly, for tissue engineering and regeneration strategies, blood vessel growth (angiogenesis) is critical to allow growth and prevent hypoxia, apoptosis, and tissue necrosis.[1,2] Current techniques to achieve angiogenesis have focused on (i) modulating inflammation using cytokines to promote a proangiogenic M2 macrophage phenotype (*e.g.*, IL-4, IL-10, MCP-1), (ii) introducing growth factors (*e.g.*, PlGF, FGF, EGF, VEGF), (iii) transplantation of mesenchymal stem cells, and (iv) induction of VEGF (vascular endothelial growth factor) production *via* gene therapy.[3−6] These approaches to achieve neovascularization have been hampered by low gene uptake, neoplasticity, immune rejection, and maladaptive inflammatory responses.[7−9] Clinical trials have met with modest success and have failed to fully recover ischemic tissue.[7,10,11] Treatment with VEGF has resulted in modest reversal of ischemia with much of the nonsequestered growth factor diffusing into the lymphatic system.[4,11−13]

Promotion of angiogenesis can be stimulated by any of the approaches described above. However, current techniques result in small, nascent vessels that fail to anastomose with host vasculature, are immature and lack supporting pericytes, or resorb too quickly—over a less than 1 week period.[3,14] Successful angiogenic materials will overcome these problems and result in (1) the development of mature vessels with a pericyte and/or muscular wall that are well connected to the host vasculature, (2) the retention of these vessels for long time periods, and (3) eventual resorption of the introduced material coupled with functional recovery of the associated tissue. We hypothesize that treatment with a specially designed multidomain peptide (MDP) sequence conjugated with a VEGF mimic will promote angiogenesis by prolonged stimuli presentation and residence time *in situ*.

MDPs are a class of peptide-based self-assembling supramolecular structures. MDPs consist of terminally charged residues that flank alternating hydrophilic and hydrophobic residues. These facial amphiphiles associate into bilayers of antiparallel β-sheets (Figure 1A). The MDPs in DI water

* Address correspondence to jdh@rice.edu.

Received for review November 17, 2014 and accepted January 5, 2015.

Published online January 13, 2015
10.1021/nn506544b

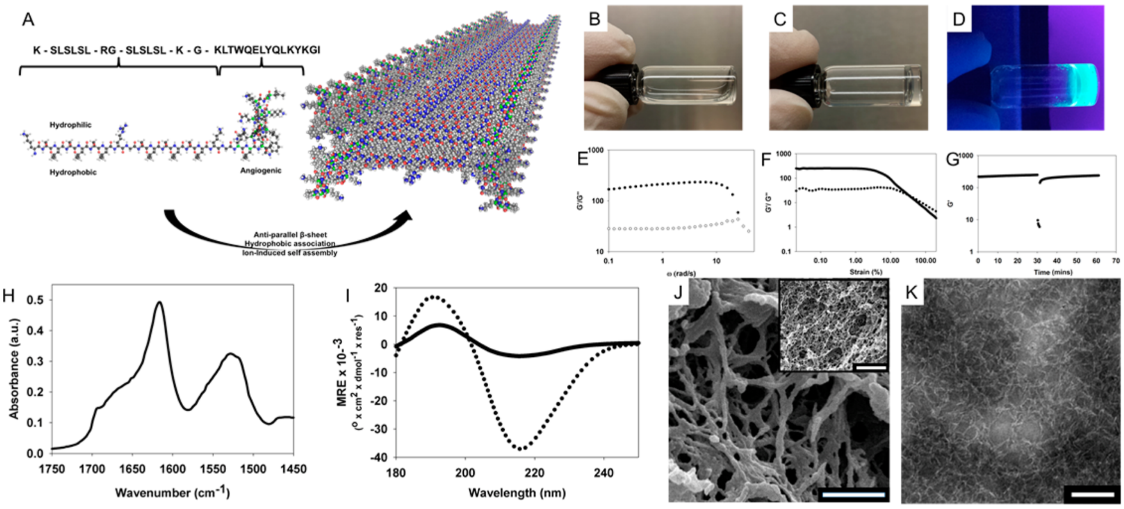

Figure 1. Physical characterization of SLanc. (A) Multidomain peptides were engineered to self-assemble, biodegrade, and present bioactive moieties. (B) SLanc peptides form a viscous solution in 298 mM sucrose (C) that gel upon the addition of anions. (D) Fluorescent carboxyfluorescein-modified SLanc (F-SLanc) was added to SLanc (1:100) and demonstrated facile gelation. Rheometry of 1 wt % gels showed high G' and G'' with shear thinning at high (E) strain rates and (F) high-frequency oscillation. (G) Demonstration of recovery from high shear rate, as experienced when aspirated or injected *via* a needle, of SLanc hydrogels. (H) FTIR spectrum shows characteristic amide I band (1625 cm^{-1} peak) and antiparallel (1695 cm^{-1} peak) β-sheet formation. (I) Circular dichroism shows the presence of a β-sheet supramolecular structure within a polymer structure (solid line), which is enhanced by the addition of polyvalent salts (dotted line). (J) SEM (scale bar 1 μm, inset 10 μm) and (K) TEM (scale bar 100 nm) show the nanofibrous matrix structure. For physical characterization of previously published MDPs including SL, SLc, and SLac, the reader is directed to refs 15−17 and 21−23.

form only short fibrils due to molecular frustration (like−like terminal charge repulsion). However, with the addition of multivalent ions (such as a PO_4^{3-}), charges on the terminal residues are shielded, allowing long-range fiber growth, entanglement, and hydrogel formation from low millimolar concentration solutions (see Supporting Information movie S1). While we have demonstrated gelation with monovalent ions at high concentrations,[15,16] to best simulate the physiological extracellular matrix, we chose to use PO_4^{3-}-based Hank's balanced salt solution (HBSS) for peptide gelation. Hydrophobic interactions and hydrogen bonding are the main driving forces for self-assembly. Because peptide association is based on groups of supramolecular interactions, peptides easily associate and dissociate and peptide fibers easily break and re-form. This equilibrium assembly allows the hydrogel formed from the associated fibers to shear thin and shear recover easily and allows for aspiration and needle delivery of nanofibrous hydrogels.[15,16] In summary, hydrogels that exhibit rapid shear thinning and recovery can be created by gelling peptide solutions with volume equivalents of HBSS. MDPs can be modified with cell adhesion, enzyme cleavage, and other sequence-based functionality.

In this work, we examine a series of self-assembling, nanofibrous MDPs for the promotion of angiogenesis. The base peptide sequence of the MDP used in this study is KKSLSLSLSLSLSLSLKK (named "SL" for the serine−leucine repeat). Sequences and names for peptides used in this study are listed in Table 1. Terminal lysines flank alternating hydrophilic serine

TABLE 1. Multidomain Peptides Studied

Name	Sequence
SL[a]	KKSLSLSLSLSLSLSLKK
SLc[a]	KSLSLSLRGSLSLSLK
SLac[a]	KSLSLSLRGSLSLSLKGRGDS
SLanc[a]	KSLSLSLRGSLSLSLKGKLTWQELYQLKYKGI
fSLanc[b]	fluorescein-KSLSLSLRGSLSLSLKGKLTWQELYQLKYKGI

[a] N-terminally acetylated and C-terminally amidated. [b] C-terminally amidated. MMP2 cleavage site highlighted in red; cell adhesion sequence highlighted in blue; VEGF mimic highlighted in green.

and hydrophobic leucine.[16−18] Three additional MDPs are studied which add functionality to this basic self-assembling peptide: KSLSLS**LRG**SLSLSLK[17] (named "SLc" for the basic SL repeat which now includes an enzyme cleavage site, c), KSLSLS**LRG**SLSLSLKG**RGDS**[17] (named "SLac" for the basic SL repeat which is augmented by both an enzyme cleavage site, c, and a cell adhesion sequence, a), and KSLSLS**LRG**SLSLSLKG-**KLTWQELYQLKYKGI** (named "SLanc" for the basic SL repeat which is augmented by both an enzyme cleavage site, c, and an angiogenic sequence, an). This last peptide, SLanc, incorporates a recently described angiogenic VEGF-165 mimic[19,20] to the C-terminus of SLc. Work from our group and others have demonstrated that MDP modification with both small and large peptides maintains β-sheet structure and fiber-forming propensity.[17,21−24] Conjugation of small peptide mimics onto the base peptide chain which drives fiber self-assembly has the effect of resulting in extremely high molar epitope presentation, potentially promoting VEGF receptor activation, dimerization, clustering, and

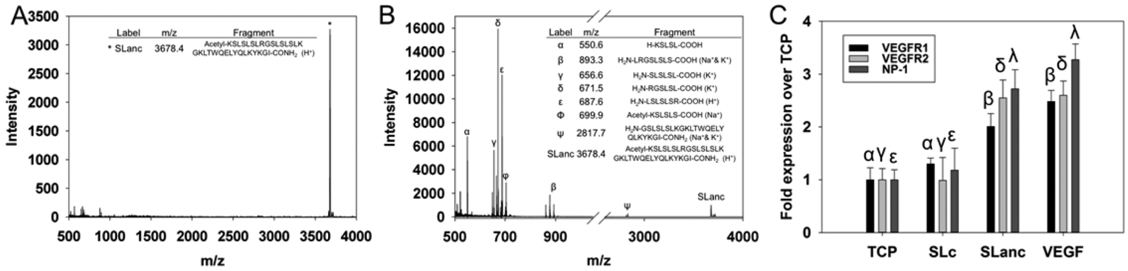

Figure 2. *In vitro* biochemical response. Controlled degradation of SLanc shown by MALDI mass spectrometry of intact SLanc before (A) and cleavage fragments after incubation with MMP-2 (B). Activation of VEGF receptors shown by PCR of VEGFR-1/2 and NP-1 interaction with different peptides or VEGF positive control. Similar Greek letters indicate no statistically significant difference for each receptor (*$p < 0.01$).

intracellular angiogenic signaling at the site of nanofibrous hydrogel delivery.[6,25−27] Furthermore, the built-in cleavage sequence in our MDPs allows for long-range diffusion of the angiogenic signal upon enzymatic degradation that may be valuable in recruiting necessary cells.

RESULTS AND DISCUSSION

Physical and Structural Characterization of SLanc. SLanc has chemical and physical characteristics that are comparable to previously published multidomain peptides. The peptide can be dissolved in deionized water but upon mixing with negatively charged multivalent ions undergoes rapid hydrogel formation (Figure 1B,C). Carboxyfluorescein-conjugated SLanc (F-SLanc) can be used to dope SLanc, yielding fluorescent gels (Figure 1D). Rheological characterization of the nanofibrous peptide hydrogel showed responsivity to high-frequency shear, with gels liquefying (inversion of G' and G'') at about 15 rad/s (Figure 1E). Further, gels demonstrate plastic strain shearing at about 20% strain (Figure 1F). To demonstrate syringe aspiration and delivery, hydrogels were sheared at high strain (100% strain) for 1 min and then returned to a low strain (1% strain). Hydrogels recover greater than 95% of their storage moduli within seconds of returning to low strain (Figure 1G), comparable or somewhat more rapid than previously reported MDPs. This quantitative assessment is borne out by qualitative tests which demonstrate that the peptide hydrogel can be easily aspirated and dispensed using needles as small as 30 gauge, resulting in a well-formed hydrogel immediately after dispensing. Similar to previously published MDPs, SLanc displays characteristic circular dichroism (CD)[16,23] and Fourier transform infrared (FTIR) spectra which suggest self-assembly into antiparallel β-sheets (Figure 1H,I). SEM and TEM of SLanc show a nanofibrous hydrogel scaffold (Figure 1J,K).

Chemical Functionality of SLanc. Chemical moieties introduced into the peptide sequence can tailor the host response to materials. In the design of SLanc, a protease cleavage sequence was introduced into the central peptide backbone. This sequence is designed to be cleaved specifically with MMP-2, which is secreted by a host of infiltrating cells ranging from macrophages to fibroblasts. *In vitro* demonstration of physiological degradation of SLanc with the addition of MMP-2 yields a variety of peptide fragments around the cleavage site (Figure 2A,B) as anticipated.[17] Similar MDPs with cleavable sequences have been characterized.[15,17] As detailed above, additional functionality was afforded to SLanc to enhance angiogenesis by conjugation of a peptide mimic derived from VEGF-165.[20] HUVEC vasculogenic receptor activation was determined by PCR. VEGFR1, VEGFR2, and NP-1 receptor activation for SLanc was similar to the positive control, VEGF-doped media. In contrast, SLc showed less activation and was similar to the negative control, tissue culture plastic (Figure 2C).[19] These chemical, rheological, structural, and biochemical data demonstrate that SLanc is an injectable self-assembling nanofibrous biodegradable scaffold, capable of activating vasculogenic receptors.

Cytocompatibility of SLanc. Multidomain peptides SL, SLc, SLac, and SLanc were assayed for cytocompatibility. First, human mesenchymal stem cells (hMSCs) were seeded onto hydrogel scaffolds. Cells showed increased adhesion to SLanc over the unfunctionalized SL but was comparable to SLc. Surprisingly, SLanc showed similar cell adhesion to SLac which contains the fibronectin-derived cell adhesion sequence RGDS (Figure 3A−F).

Next, the scaffolds' pro-inflammatory potential was evaluated. Their proclivity to activate a pro-inflammatory M1 macrophage phenotype was assayed by incubating THP-1 cells atop scaffolds. TNF-α and IL-1β levels were determined by ELISA for all scaffolds, and MDP hydrogels were found to be significantly lower than cells treated with lipopolysacharide and similar to commercially available scaffolds such as Puramatrix and Matrigel (Figure 3G,H). Finally, HUVEC cytocompatibility was evaluated to determine the ability of endothelial cells to proliferate on scaffolds. Endothelial cells showed proliferation on SLanc scaffolds similar to that on SLac scaffolds. Scratch wound healing and cellular infiltration into scratch wounds in response to SLanc showed wound healing similar to that of SLac (Figure 3J−L).

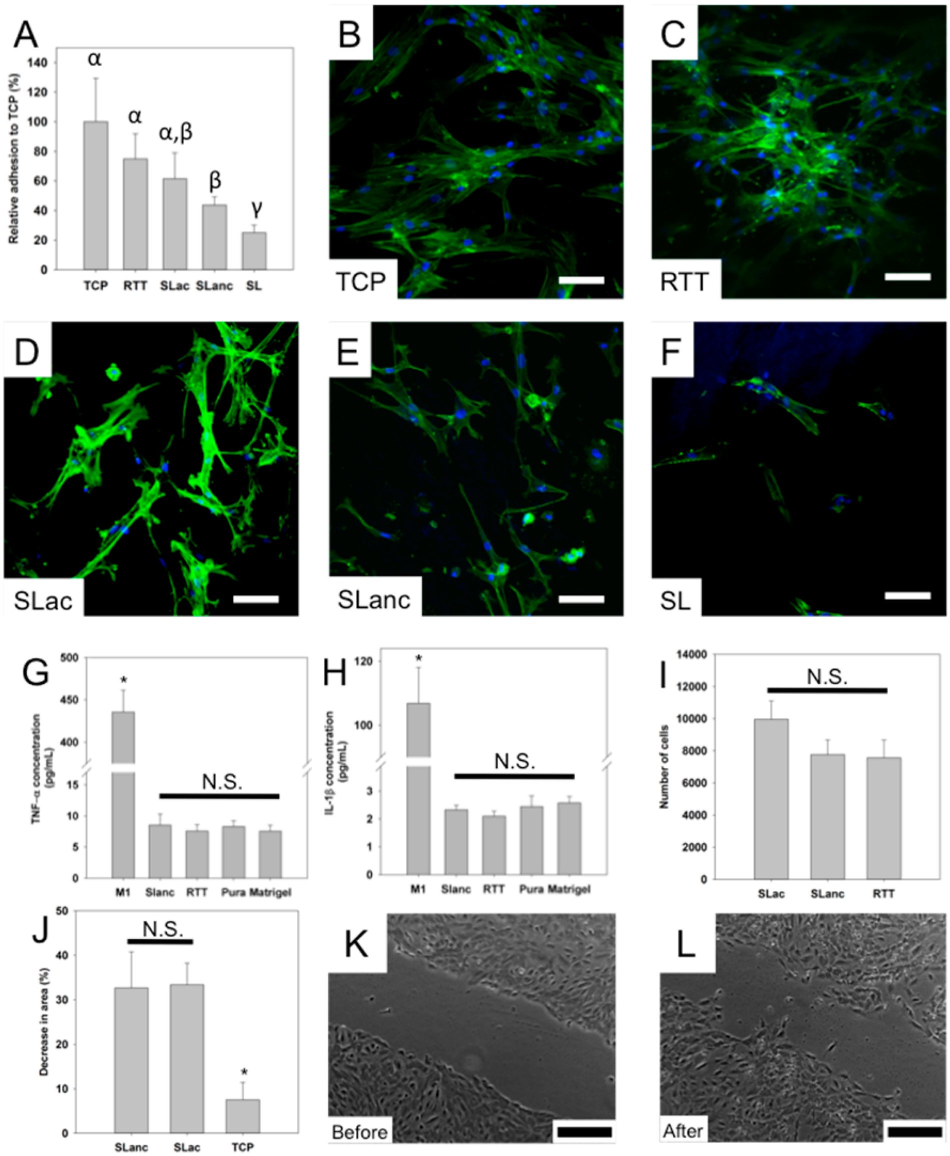

Figure 3. Cell adhesion and scratch wound healing on scaffolds. With respect to hMSCs, (A) TCP showed greatest adhesion, while RGD-modified SLac and angiogenic SLanc showed similar cell adhesion. Representative images of hMSC adhered and spread on all scaffolds: (B) TCP, (C) RTT, (D) SLac, (E) SLanc, and (F) SL; scale bar 100 μm. Inflammatory potential of scaffolds measured by incubating THP-1 cells atop scaffolds and measuring TNF-α (G) and IL-1β (H) secretion. Quantification of HUVEC adhesion on scaffolds showed (I) HUVEC proliferated to a similar extent on all hydrogel material surfaces after 4 days. Migration of HUVEC into a scratch wound with a soluble peptide stimulus was measured (J). Conditions were in low FBS (0.5%) media after 18 h. SLac and SLanc showed significantly higher proliferation than TCP. Representative images of a SLanc healed scratch wound are shown (K) before and (L) after; scale bar 250 μm. Similar Greek letters indicate no statistically significant difference (*p < 0.01).

While the results underscore the apparent effect of the GRGDS moiety on cell adhesion as we have seen previously,[17,21] other factors may be involved in hMSC adhesion such as cell-matrix interactions. Further, with respect to hMSCs, SLanc did show a significant increase in cell adhesion over SL scaffolds alone, suggesting the potential for the addition of the QK domain to improve cell adhesion. In HUVEC adhesion studies, we noted that both SLac and SLanc scaffolds offer similar cell adhesivity as compared to rat tail tendon collagen gels. In the case of SLac and rat tail tendon collagen scaffolds, HUVECs are being activated by their integrin receptors promoting cell adhesion. In the case of SLanc scaffolds, VEGFR-1, VEGFR-2, and NP-1 receptors are upregulated, as shown in Figure 2, promoting cellular proliferation.

***In Vivo* Angiogenic Response of Multidomain Peptides.** In modeled diseases, such as ligated femoral artery ischemic limb wounds or myocardial infarction, several host tissue responses are activated. From secretion of mediators of inflammation such as MCP-1, IL-4, IL-10, SDF-1, and GCSF to growth factors such as VEGF, FGF, and EGF, extrinsic factors can drastically influence performance of materials.[1,3,4,10,14] These types of

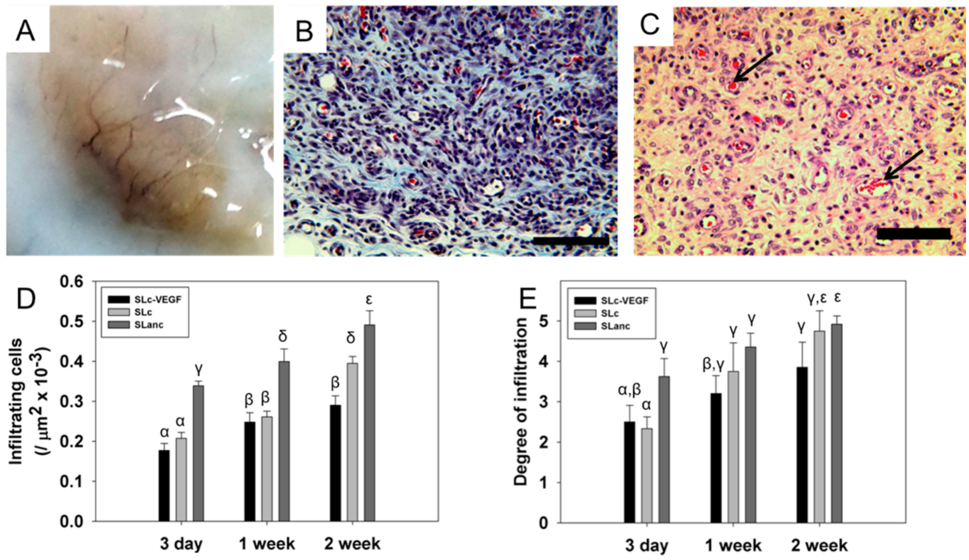

Figure 4. Cellular infiltration and angiogenesis within scaffolds. (A) Upon explant, SLanc scaffolds showed visible macroscale vessels at 7 days. (B) Masson's Trichrome and (C) H&E staining show rapid infiltration of scaffolds and presence of blood vessels with red blood cells (arrows) at 1 week; scale bar 100 μm. A magnified image of the blood vessel clearly showing RBCs flowing through is shown in Figure S3. Control and 3 day time points shown in Figures S1 and S2. (D) SLanc scaffolds show significantly greater cellular infiltrate toward the center of scaffolds and (E) degree of infiltration, compared to SLc or SLc-VEGF. Similar Greek letters indicate no statistically significant difference ($p < 0.01$).

responses are generated in all oxygen-deprived tissue and make isolation of the effect of putatively angiogenic materials difficult. Because of this, we wanted to evaluate our scaffolds without the influence of these native disease and injury-stimulated responses. Therefore, a simple subcutaneous injection of the MDP scaffold was used. This model allows us to evaluate (1) the ease of syringe-directed delivery of our shear thinning and recovering hydrogels, (2) cellular infiltration from the host, (3) any inflammatory response and/or fibrous encapsulation, as well as (4) angiogenesis within the syringe-delivered nanofibrous hydrogel.

Nanofibrous MDP hydrogels SL, SLc, and SLanc were prepared at a final peptide concentration of 1% by weight and were easily injected subcutaneously in rats using a 30 gauge needle. The bolus of hydrogel was evaluated at 3, 7, 14, and 21 days. Hydrogels of MDP remained localized and easily identifiable through 14 days. At 21 days, hydrogels were no longer readily apparent. Both SLc and SLanc hydrogels showed remarkably rapid and thorough cellular infiltration, regardless of sequence, even after only 3 days subsequent to injection (Figure S1). Many of these cells were found to be CD68$^+$ macrophages (Figure S4). In all cases, there was a distinct lack of fibrous encapsulation or walling off of the injected implants. This suggests that communication from within the injectable hydrogels to the extracellular matrix and *vice versa* would be possible. Interestingly, as indicated by SEM and TEM, these scaffolds have pores on the nanometer size scale, and as such, infiltration of cells must be due to either proteolysis of the peptide scaffold or molecular reorganization by the infiltrating cells. In addition to the lack of fibrous encapsulation, the tissue surrounding the MDP hydrogels was not red or swollen and rats did not display any unusual behavior suggestive of a negative inflammatory response.

In the case of SLanc, gross morphological analyses of explants showed a large number of blood vessels surrounding the implant (Figure 4A) compared to implants of SLc (Figure S1), which showed no visible vasculature. Vessels and extracellular matrix syntheses were further identified using Masson's Trichrome staining (Figure 4B). H&E staining of injected scaffolds showed that SLc and SLc loaded with VEGF showed similar extent of cellular infiltration (depth of infiltration into the bolus), but both with significantly fewer cells compared to SLanc scaffolds (Figure 4C–E and Supporting Information Figures S1B,C, S2, and S3). VEGF injected in phosphate buffered saline and Puramatrix subcutaneous injections could not be identified at the 3 day, or subsequent time points, which suggests that they were rapidly resorbed and had no lasting effect on the surrounding tissue. SLanc scaffolds contained small nascent vessels at day 3, and by day 7, they contained an amazingly large number of very mature vessels as identified by their staining with Nestin$^+$, α-SMA$^+$, and CD31$^+$ (Figure 5A and Figure S3). These mature vessels persist at the 14 day time point (Figure S5). Blood vessels in H&E-stained sections of SLanc implants were as large as 50 μm in diameter and contained numerous red blood cells (Figure S3). Further, CD45$^+$ hematopoietic cells were noted within vWF$^+$ vessels, suggesting patent, perfused, and mature neovessels, which were quantified (Figure 5B–D).

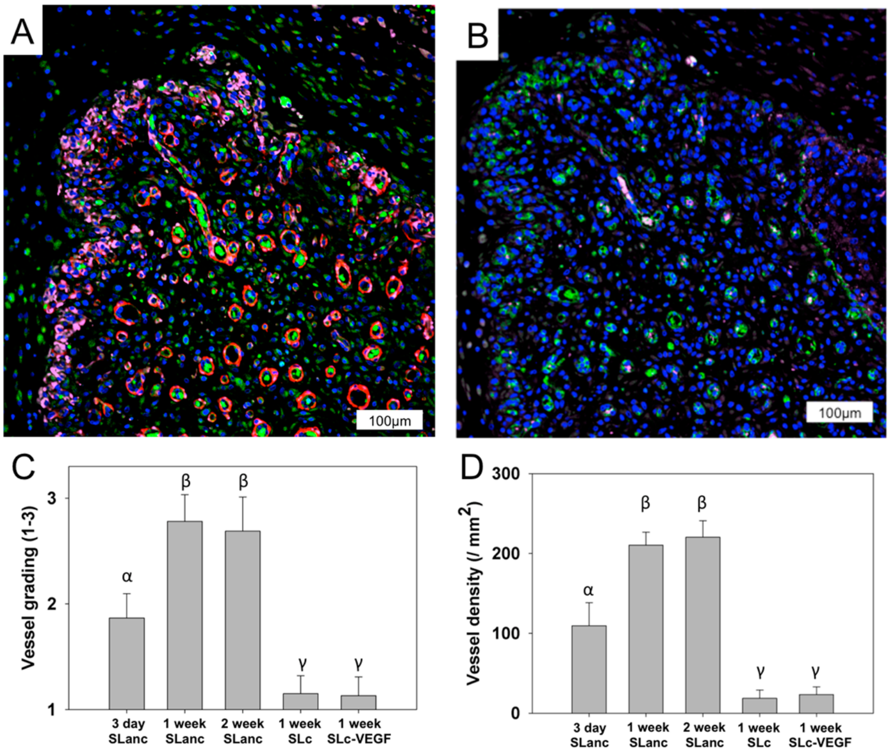

Figure 5. ***In vivo*** **efficacy of SLanc in promoting angiogenesis, venulo/arteriolo genesis. (A) Immunostaining of cells from hematopoietic and mesenchymal origin showing extensive infiltration of pericyte-like cells (purple, Nestin$^+$), which costain with SMC (red, α-SMA$^+$), surrounding endothelial cells in large stable microvessels and circulating cells (green, CD31$^+$); select region magnified in Figure S4 and controls in S5. (B) Perfusion of vessel was confirmed by observation of circulating cells of hematopoietic origin (purple, CD45$^+$) in endothelial lined (green, vWF$^+$) vessels. (C) Vascular tube formation and (D) vessel maturity were significantly higher in SLanc compared to SLc/SLc-VEGF controls. Similar Greek letters indicate no statistically significant difference ($p < 0.01$).**

Studies with VEGF-doped SLc resulted in minimal angiogenesis (Figure S1). Muted angiogenesis may be due to insufficient VEGF angiogenic epitope concentration and rapid diffusion. VEGF-loaded scaffolds presented 100 ng of recombinant protein (13 nM) within scaffolds. In comparison, the VEGF mimetic has an effective concentration of 2.7 mM, 27 000× higher than the VEGF loading and much higher than can reasonably be cost-effective when using the full VEGF protein. Additionally, while the VEGF loaded in SLc scaffolds is free to diffuse away in a matter of hours, the SLanc hydrogel persists with its VEGF mimic signal for weeks. The combination of concentration and persistence over time leads to the remarkable angiogenic response observed.

All tested MDP hydrogels show extensive and rapid host cell infiltration, and with a lack of fibrous encapsulation, these cells of immune, hematopeotic, and mesenchymal origin have the potential to provide an excellent niche for tissue regeneration.[1,3] In SLanc, this results in a robust angiogenic response driven by the VEGF mimic which recruits endothelial feeders from existing vessels. Pericytic cells enhance stability of growing vessels in a paracrine fashion, providing adequate support for generation of arterioles.[1,2,28] While these vessels are robust and patent, at the 1 week and 2 week time points, implants could not be identified in gross histology (Figure S6) at 3 weeks, suggesting that they are subsequently resorbed by the host as there is no need for extensive vascularization in the fascia. The importance of this design strategy is underscored by the rapid development of angiogenic networks around the implants (within 3 days), stable vessels within implants (within 7 days), and resorption of superfluous vessels and implants without development of hematomas or hemorrhaging (within 3 weeks).

Comparison to Previous Strategies and Proposed Mechanism. A variety of VEGF mimics have been used previously.[6,19,20,25,27] Since its identification and isolation in 2005,[20] this VEGF-165 mimic, frequently named QK, has shown to be highly conserved and stable in secondary structure and activates a host of VEGF receptors.[19,20,29] Stemming from this, several groups have conjugated QK to surfaces,[29] PEG hydrogels,[30,31] and self-assembling peptides.[27,32] These studies affirm that QK stimulates VEGF receptor activation and dimerization and can potentially stimulate tissue regeneration.[27,30,33] However, these studies have yet to achieve the required criteria for functional angiogenic vessel development: (1) stabilization of vessels with pericytes/smooth muscle cells, (2) retention of vessels, and (3) integration or resorption after 2−3 weeks. SLanc, however, shows rapid angiogenesis with the development of mature vessels in just 7 days.

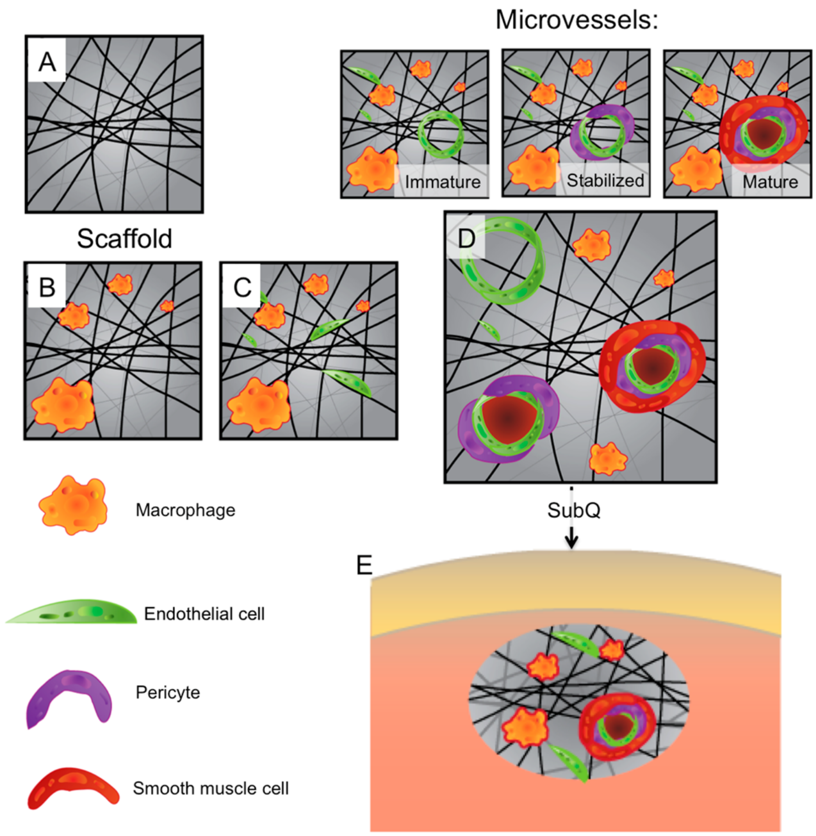

Figure 6. Proposed mechanism of healing. (A) SLanc scaffolds form nanofibrous hydrogels. (B) Scaffolds rapidly infiltrate with macrophages. (C) Hydrophobic and ionically bound SLanc at the periphery of scaffolds recruits endothelial cells to infiltrated scaffolds, which interact with current infiltrate to form blood vessels. (D) Subcutaneous and intramuscular implanted scaffolds rapidly form CD31$^+$, vWF$^+$, Nestin$^+$, and α-SMA$^+$ microvessels that have CD45$^+$ cells that flow through their lumen. Images above (D) show progression of vessels from immature (EC only) to stabilized (EC + pericyte) to mature (EC + pericyte + SMC). (E) Neovessels in the subcutaneous model resorb since they do not anastamose injured/damaged vessels.

This rapid response may be particularly suitable for translation into clinically viable treatments.[27,34−37]

In the design of this study, we assayed the effects that SLanc had on the chemistry and self-assembly of an MDP and its effects on cells *in vitro* and *in vivo*. We show that SLanc scaffolds still formed β-sheet-based nanofibrous hydrogels and maintained desirable material properties, while stimulating VEGF receptors and being susceptible to cleavage by MMP-2. *In vitro* results confirmed cytocompatibility. Subcutaneous injections into rats demonstrate rapid infiltration by cells and development of stable perfused vasculature within 7 days that resorb by 3 weeks. Infiltrating cells preload scaffolds with necessary vascular support cells, as seen in 3 day histology. We postulate that a small amount of the VEGF mimic diffuses away from the hydrogel bolus by either simple equilibrium of an intact SLanc peptide or subsequent proteolysis of the MMP-2 cleavage site. This signal can diffuse toward native vasculature, prompting budding and growth of feeder vessels to the implant. The bolus of the VEGF mimic can then promote robust angiogenesis into the implant. Due to the lack of a fibrous capsule, communication inside and outside scaffolds is readily available. Finally, infiltrating vessels mature by support cells, leading to perfused microvessels (Figure 5B), shown schematically in Figure 6. This unprecedented rate of angiogenesis with development of mature vessels in a subcutaneous model (Figure 5) promotes the use of these scaffolds and presents a paradigm in clinically available treatments for ischemic tissue disease.

CONCLUSION

Effective promotion of angiogenic stimuli is a critical factor in nearly all efforts toward tissue engineering and regeneration and is particularly critical in systems of acute and chronic ischemia. In this study, a self-assembled, nanofibrous hydrogel of a multidomain peptide named SLanc presents a VEGF-165 peptide mimic. SLanc is cytocompatible and is cleaved by MMP2, and the VEGF mimic activates VEGFR-1, VEGFR2, and NP-1 receptors *in vitro*. SLanc can be delivered by simple syringe injection, and the hydrogel bolus is rapidly infiltrated with host cells, has no fibrous encapsulation, and has excellent tissue integration. By day 7, these hydrogels have large and numerous microvessels which stain positive for vWF, CD31, α-SMA, and Nestin. The results of this study suggest the potential for this angiogenic peptide to be used in a broad range of tissue regeneration strategies where vascularization is required and, in particular, for therapeutic revascularization postmyocardial infarction, stroke, and other ischemic tissue diseases.

EXPERIMENTAL SECTION

Peptide Preparation and *In Vitro* Characterization. Multidomain peptides were synthesized, purified, and dissolved aseptically at 20 mg/mL in sterile 298 mM sucrose. Gelation of the peptide was achieved by addition of equivalent volumes of pH 7.4 buffer with 1× PBS or HBSS. Detailed synthesis methods and *in vitro* chemical (mass spec, VEGFR binding, FTIR), mechanical (rheology), thermal (CD), microstructural characterization (SEM and TEM), cellular compatibility (HUVEC, hMSCs), and pro-inflammatory response (THP-1) are described in the Supporting Information.

***In Vivo* Characterization.** All experiments were approved by the Rice University Institutional Animal Care and Use Committee. Female Wistar rats (225−250 g) were injected subcutaneously in the dorsal aspect with 200 μL of peptide scaffolds. At prescribed time points, dorsal skin was removed and processed into paraffin blocks. Samples were processed for routine histology and immunofluorescence staining, detailed in the supplementary methods. Detailed methods and surgical procedures are presented in the Supporting Information.

Conflict of Interest: The authors declare no competing financial interest.

Acknowledgment. The work presented in this paper was supported by grants from the Robert A. Welch Foundation for J.D.H. (Grant C1557), and the National Institute of Health for J.D.H. (R01 DE021798) and V.A.K. (F32 DE023696). The authors would like to thank the Breast Cancer Pathology Core at the Baylor College of Medicine for assistance with histomorphometry, and Paul Derry and Dr. Jorge Wong at Rice University for assistance with Figure 6 and movie S1, respectively. The experiments were designed by V.A.K., A.A.J., and J.D.H., carried out by V.A.K., N.L.T., B.K.W., A.A.J., S.S., M.K.K., and N.C.W., and interpreted by V.A.K., N.C.W., and J.D.H. The manuscript was written by V.A.K., N.C.W., and J.D.H.

Supporting Information Available: Detailed methods are presented. A movie showing schematic self-assembly of SLanc is shown (movie S1). Self-assembly of proangiogenic multidomain peptides. Further *in vivo* characterization is shown (Figure S1). Control subcutaneous implants (Figure S2). SLanc infiltration (Figure S3). High-magnification image SLanc implant (Figure S4). Details of SLanc vessel morphology and macrophage infiltration (Figure S5). Phenotypic characterization of the infiltrate. This material is available free of charge *via* the Internet at http://pubs.acs.org.

REFERENCES AND NOTES

1. Radecki, R. P. Acute Ischemic Stroke and Timing of Treatment. *JAMA* **2013**, *310*, 1855–1856.
2. Heusch, G.; Libby, P.; Gersh, B.; Yellon, D.; Bohm, M.; Lopaschuk, G.; Opie, L. Cardiovascular Remodelling in Coronary Artery Disease and Heart Failure. *Lancet* **2014**, *383*, 1933–1943.
3. Courties, G.; Moskowitz, M. A.; Nahrendorf, M. The Innate Immune System after Ischemic Injury: Lessons To Be Learned from the Heart and Brain. *JAMA Neurol.* **2014**, *71*, 233–236.
4. Sun, Q.; Silva, E. A.; Wang, A.; Fritton, J. C.; Mooney, D. J.; Schaffler, M. B.; Grossman, P. M.; Rajagopalan, S. Sustained Release of Multiple Growth Factors from Injectable Polymeric System as a Novel Therapeutic Approach towards Angiogenesis. *Pharm. Res.* **2010**, *27*, 264–271.
5. Mohsin, S.; Wu, J. C.; Sussman, M. A. Predicting the Future with Stem Cells. *Circulation* **2014**, *129*, 136–138.
6. Phelps, E. A.; Garcia, A. J. Engineering More Than a Cell: Vascularization Strategies in Tissue Engineering. *Curr. Opin. Biotechnol.* **2010**, *21*, 704–709.
7. Giacca, M.; Zacchigna, S. VEGF Gene Therapy: Therapeutic Angiogenesis in the Clinic and Beyond. *Gene Ther.* **2012**, *19*, 622–629.
8. Lu, J.; Pompili, V. J.; Das, H. Neovascularization and Hematopoietic Stem Cells. *Cell Biochem. Biophys.* **2013**, *67*, 235–245.
9. Katare, R.; Stroemer, P.; Hicks, C.; Stevanato, L.; Patel, S.; Corteling, R.; Miljan, E.; Vishnubhatla, I.; Sinden, J.; Madeddu, P. Clinical-Grade Human Neural Stem Cells Promote Reparative Neovascularization in Mouse Models of Hindlimb Ischemia. *Arterioscler., Thromb., Vasc. Biol.* **2014**, *34*, 408–418.
10. Stewart, D. J.; Kutryk, M. J.; Fitchett, D.; Freeman, M.; Camack, N.; Su, Y.; Della Siega, A.; Bilodeau, L.; Burton, J. R.; Proulx, G.; Radhakrishnan, S. VEGF Gene Therapy Fails To Improve Perfusion of Ischemic Myocardium in Patients with Advanced Coronary Disease: Results of the Northern Trial. *Mol. Ther.* **2009**, *17*, 1109–1115.
11. Simon-Yarza, T.; Formiga, F. R.; Tamayo, E.; Pelacho, B.; Prosper, F.; Blanco-Prieto, M. J. Vascular Endothelial Growth Factor-Delivery Systems for Cardiac Repair: An Overview. *Theranostics* **2012**, *2*, 541–552.
12. Webber, M. J.; Han, X.; Murthy, S. N.; Rajangam, K.; Stupp, S. I.; Lomasney, J. W. Capturing the Stem Cell Paracrine Effect Using Heparin-Presenting Nanofibres To Treat Cardiovascular Diseases. *J. Tissue Eng. Regener. Med.* **2010**, *4*, 600–610.
13. Chen, R. R.; Snow, J. K.; Palmer, J. P.; Lin, A. S.; Duvall, C. L.; Guldberg, R. E.; Mooney, D. J. Host Immune Competence and Local Ischemia Affects the Functionality of Engineered Vasculature. *Microcirculation* **2007**, *14*, 77–88.
14. Grochot-Przeczek, A.; Dulak, J.; Jozkowicz, A. Therapeutic Angiogenesis for Revascularization in Peripheral Artery Disease. *Gene* **2013**, *525*, 220–228.
15. Aulisa, L.; Dong, H.; Hartgerink, J. D. Self-Assembly of Multidomain Peptides: Sequence Variation Allows Control over Cross-Linking and Viscoelasticity. *Biomacromolecules* **2009**, *10*, 2694–2698.
16. Dong, H.; Paramonov, S. E.; Aulisa, L.; Bakota, E. L.; Hartgerink, J. D. Self-Assembly of Multidomain Peptides: Balancing Molecular Frustration Controls Conformation and Nanostructure. *J. Am. Chem. Soc.* **2007**, *129*, 12468–12472.
17. Galler, K. M.; Aulisa, L.; Regan, K. R.; D'Souza, R. N.; Hartgerink, J. D. Self-Assembling Multidomain Peptide Hydrogels: Designed Susceptibility to Enzymatic Cleavage Allows Enhanced Cell Migration and Spreading. *J. Am. Chem. Soc.* **2010**, *132*, 3217–3223.
18. Galler, K. M.; Cavender, A.; Yuwono, V.; Dong, H.; Shi, S.; Schmalz, G.; Hartgerink, J. D.; D'Souza, R. N. Self-Assembling Peptide Amphiphile Nanofibers as a Scaffold for Dental Stem Cells. *Tissue Eng., Part A* **2008**, *14*, 2051–2058.
19. Santulli, G.; Ciccarelli, M.; Palumbo, G.; Campanile, A.; Galasso, G.; Ziaco, B.; Altobelli, G. G.; Cimini, V.; Piscione, F.; D'Andrea, L. D.; Pedone, C.; Trimarco, B.; Iaccarino, G. *In Vivo* Properties of the Proangiogenic Peptide QK. *J. Transl. Med.* **2009**, *7*, 41.
20. D'Andrea, L. D.; Iaccarino, G.; Fattorusso, R.; Sorriento, D.; Carannante, C.; Capasso, D.; Trimarco, B.; Pedone, C. Targeting Angiogenesis: Structural Characterization and Biological Properties of a *De Novo* Engineered VEGF Mimicking Peptide. *Proc. Natl. Acad. Sci. U.S.A.* **2005**, *102*, 14215–14220.
21. Kang, M. K.; Colombo, J. S.; D'Souza, R. N.; Hartgerink, J. D. Sequence Effects of Self-Assembling Multidomain Peptide Hydrogels on Encapsulated Shed Cells. *Biomacromolecules* **2014**, *15*, 2004–2011.
22. Bakota, E. L.; Aulisa, L.; Galler, K. M.; Hartgerink, J. D. Enzymatic Cross-Linking of a Nanofibrous Peptide Hydrogel. *Biomacromolecules* **2011**, *12*, 82–87.

23. Bakota, E. L.; Sensoy, O.; Ozgur, B.; Sayar, M.; Hartgerink, J. D. Self-Assembling Multidomain Peptide Fibers with Aromatic Cores. *Biomacromolecules* **2013**, *14*, 1370–1378.
24. Hudalla, G. A.; Sun, T.; Gasiorowski, J. Z.; Han, H.; Tian, Y. F.; Chong, A. S.; Collier, J. H. Gradated Assembly of Multiple Proteins into Supramolecular Nanomaterials. *Nat. Mater.* **2014**, *13*, 829–836.
25. Phelps, E. A.; Landazuri, N.; Thule, P. M.; Taylor, W. R.; Garcia, A. J. Bioartificial Matrices for Therapeutic Vascularization. *Proc. Natl. Acad. Sci. U.S.A.* **2010**, *107*, 3323–3328.
26. Whitaker, G. B.; Limberg, B. J.; Rosenbaum, J. S. Vascular Endothelial Growth Factor Receptor-2 and Neuropilin-1 Form a Receptor Complex That Is Responsible for the Differential Signaling Potency of VEGF(165) and VEGF(121-). *J. Biol. Chem.* **2001**, *276*, 25520–25531.
27. Webber, M. J.; Tongers, J.; Newcomb, C. J.; Marquardt, K. T.; Bauersachs, J.; Losordo, D. W.; Stupp, S. I. Supramolecular Nanostructures That Mimic VEGF as a Strategy for Ischemic Tissue Repair. *Proc. Natl. Acad. Sci. U.S.A.* **2011**, *108*, 13438–13443.
28. Sun, Q.; Chen, R. R.; Shen, Y.; Mooney, D. J.; Rajagopalan, S.; Grossman, P. M. Sustained Vascular Endothelial Growth Factor Delivery Enhances Angiogenesis and Perfusion in Ischemic Hind Limb. *Pharm. Res.* **2005**, *22*, 1110–1116.
29. Koepsel, J. T.; Nguyen, E. H.; Murphy, W. L. Differential Effects of a Soluble or Immobilized Vegfr-Binding Peptide. *Integr. Biol.* **2012**, *4*, 914–924.
30. Leslie-Barbick, J. E.; Saik, J. E.; Gould, D. J.; Dickinson, M. E.; West, J. L. The Promotion of Microvasculature Formation in Poly(ethylene glycol) Diacrylate Hydrogels by an Immobilized VEGF-Mimetic Peptide. *Biomaterials* **2011**, *32*, 5782–5789.
31. Moon, J. J.; Saik, J. E.; Poche, R. A.; Leslie-Barbick, J. E.; Lee, S. H.; Smith, A. A.; Dickinson, M. E.; West, J. L. Biomimetic Hydrogels with Pro-angiogenic Properties. *Biomaterials* **2010**, *31*, 3840–3847.
32. Liu, X.; Wang, X.; Horii, A.; Wang, X.; Qiao, L.; Zhang, S.; Cui, F. Z. *In Vivo* Studies on Angiogenic Activity of Two Designer Self-Assembling Peptide Scaffold Hydrogels in the Chicken Embryo Chorioallantoic Membrane. *Nanoscale* **2012**, *4*, 2720–2727.
33. Finetti, F.; Basile, A.; Capasso, D.; Di Gaetano, S.; Di Stasi, R.; Pascale, M.; Turco, C. M.; Ziche, M.; Morbidelli, L.; D'Andrea, L. D. Functional and Pharmacological Characterization of a VEGF Mimetic Peptide on Reparative Angiogenesis. *Biochem. Pharmacol.* **2012**, *84*, 303–311.
34. Liu, Q.; Xi, Y.; Terry, T.; So, S. P.; Mohite, A.; Zhang, J.; Wu, G.; Liu, X.; Cheng, J.; Ruan, K. H.; Willerson, J. T.; Dixon, R. A. Engineered Endothelial Progenitor Cells That Overexpress Prostacyclin Protect Vascular Cells. *J. Cell. Physiol.* **2012**, *227*, 2907–2916.
35. Liu, X.; Terry, T.; Pan, S.; Yang, Z.; Willerson, J. T.; Dixon, R. A.; Liu, Q. Osmotic Drug Delivery to Ischemic Hindlimbs and Perfusion of Vasculature with Microfil for Micro-computed Tomography Imaging. *J. Visualized Exp.* **2013**, e50364.
36. Liu, X.; Terry, T.; Pan, S.; Yang, Z.; Willerson, J. T.; Dixon, R. A.; Liu, Q. Targeted Delivery of Carbaprostacyclin to Ischemic Hindlimbs Enhances Adaptive Remodeling of the Microvascular Network. *Hypertension* **2013**, *61*, 1036–1043.
37. Terry, T.; Chen, Z.; Dixon, R. A.; Vanderslice, P.; Zoldhelyi, P.; Willerson, J. T.; Liu, Q. Cd34(+)/M-Cadherin(+) Bone Marrow Progenitor Cells Promote Arteriogenesis in Ischemic Hindlimbs of Apoe(−)/(−) Mice. *PLoS One* **2011**, *6*, e20673.